Maderas-Cienc Tecnol 24(2022):2, 1-20
Ahead of Print: Accepted Authors Version

DOI:10.4067/S0718-221X2022005XXXXXX

MASS TRANSFER PROPERTIES OF *ACACIA MANGIUM* PLANTATION WOOD

Ha Tien Manh[1*], Adam L. Redman[2], Chuong Pham Van[3], Bui Duy Ngoc[1]

[1] Research Institute of Forest Industries, Vietnamese Academy of Forest Sciences, Bac Tu Liem, Hanoi, Vietnam.

[2] Queensland Department of Agriculture and Fisheries, Horticulture and Forestry Science, Salisbury Research Facility, Salisbury, Queensland, Australia.

[3] Vietnam National University of Forestry, Xuan Mai, Chuong My, Hanoi, Vietnam.

***Corresponding author:** hatienmanhfsiv@gmail.com

Received: June 02, 2020.

Accepted: September 20, 2021

Posted online: September 21, 2021

ABSTRACT

This study investigated the mass transfer properties (permeability and mass diffusivity) in the longitudinal, radial and tangential directions of plantation-grown *Acacia mangium* in Vinh Phuc province, northeast, Vietnam. These properties will be used to complement a conventional drying model in the future. Measurements of gas and liquid permeability were performed using a Porometer (POROLUX^{TM}1000). Mass diffusivity was determined in a constant humidity and temperature chamber using PVC-CHA vaporimeters. Results showed the gas permeability was significant higher than liquid with the descending order of longitudinal, radial, and tangential directions. The permeability anisotropy ratios from the longitudinal to transverse directions of *Acacia mangium* were much lower than other published species. However, the obvious anisotropy ratios from radial to tangential for both permeability and diffusivity, is one of concerns as they can exacerbate defects during drying. Besides, the high permeability and diffusivity of *Acacia mangium* compared to some other species reported compounds its relatively fast drying rate.

Keywords: *Acacia mangium*, anisotropy, diffusivity, mass transfer, permeability.

INTRODUCTION

Vietnam has a large expanding area of plantation forests for over 30 years and the majority of plantation species harvested are acacias. In 1992, 7,2 % of the 913466 ha of planted forest area were acacia species: *Acacia auriculiformis* (43110 ha) and *Acacia mangium* (23021 ha) (De Jong *et al.* 2006). In 2013, the planted forest area increased by 3,89 times, reaching 3556294 ha (Tuan 2014). Among them, the acacia plantation area is about 1,1 million ha (31 %), with 600000 ha of *A. mangium*, mainly in the north, 400000 ha of clonal acacia hybrid (*A. mangium* × *auriculiformis*), 90000 ha of *A. auriculiformis,* and 5000 ha of *A. crassicarpa* (Harwood and Nambiar 2014). In 2019, the planted forest area was 4316786 ha, of which the acacia species area still constitute a large proportion (Tuan 2020).

In Vietnam, the export turnover of raw wood goods, especially chips, logs, and sawn timber makes a large proportion of total wood products. In 2018, the export value was 2,19 billion US dollars, accounting for 28,8 % of total export turnovers of wood and wood products. Meanwhile logs and sawn timber materials are imported to provide companies for further processing. Transforming the harvesting structure of plantations from young timber to large timber to supply raw materials for the processing industry to raise the added value of planted forest timber has been an important orientation of the government and forestry departments.

In order to create high quality products from wood, wood drying is an important and mandatory stage in the manufacturing process. There are various methods to perform the drying process including conventional kilns, direct or indirect heating kilns, dehumidifier kilns, solar kilns, microwave drying units, and vacuum kilns (Phonetip 2018). These drying methods require to control the occurrence of defects during the drying process. This means maintaining a balance between the rate of evaporation of surface moisture and the rate of moisture movement from the interior to the surface of the wood. An

effective solution is to use an optimized drying schedule in controlling temperature, relative humidity and airflow under atmospheric pressure (Redman *et al.* 2017).

The use of mathematical models to optimize the wood drying process is considered by many researchers to be a reliable and cost-effective solution since it does not require spending a lot of time and money on experimental drying batches. A mathematical model can be used to understand and predict drying time and wood quality (Haque 2002). In addition, an accurate mathematical model will be effectively used to evaluate the effect of drying regimes on the drying behavior of wood (Yuniarti *et al.* 2018).

To optimize the drying process using a mathematical model, a good understanding of the wood and its drying behavior is required (Redman *et al.* 2017). Several wood properties need to be measured to provide data for developing an accurate drying model. In particular, permeability and water-vapour diffusivity are the key parameters of mass transfer data of the drying model (Redman *et al.* 2012).

This paper provides results on the measurement of the gas and liquid permeability, which determine mass flow due to the pressure difference; and the water-vapour diffusivity, which determine mass flow due to the concentration difference, of *A. mangium* to provide input data for later drying model.

MATERIALS AND METHODS

Materials

The material used for the study, 9-year old *A. mangium* logs, was harvested in Ngoc Thanh Commune, Phuc Yen City, Vinh Phuc Province, Vietnam. Each log was sawn into boards with dimensions 1000 mm x 80 mm x 27 mm (L, W, T dimensions). These 200 defect-free boards were selected to dry together from 50 % to 20 % moisture content during 50 days in a batch of solar kiln located at the Research Institute of Forest Industries, Vietnamese Academy of Forest Sciences, Hanoi, Vietnam. The temperature and relative humidity (RH) of this drying batch depend on weather. The temperature was

highest on clear sunny day (48 ºC) and lowest at the night (15 ºC) and the RH was 73 % and 98 % respectively. The air flow was 2 m/s.

Among them, 10 defect-free boards (5 quarter-sawn and 5 back-sawn boards) with dimensions 300 mm x 75 mm x 25 mm (L, R, T and L, T, R orientations, respectively) were prepared to transport to Salisbury Research Facility, Department of Agriculture and Fisheries, Queensland, Australia, for mass transfer properties investigation. These 10 boards were then sawn into three sections (Figure 1). From the end of the boards, a 70 mm long sawn section was removed and a pair of 23 mm diameter cylinders were cored through the surface using a 28 mm hole-saw. Each core was cut into two equal thickness pieces using a band-saw and was router planed to 10 mm thickness, to produce 20 tangential and 20 radial permeability samples (right side of the diagram). Sixty longitudinal permeability and 20 longitudinal diffusivity samples were taken along the grain from these sections. The dimensions and preparation of longitudinal permeability samples were same as those used to determine transverse permeability. The longitudinal diffusivity samples were 19 mm in diameter and 17 mm in long cylinders. Those were cored using a 24 mm hole-saw, cut by a band-saw, and router planed. All of permeability samples were divided into 2 equal numbers to determine gas and liquid permeability. Each 80 mm long sawn section on the left side of the diagram was cored through the surface using a 79 mm diameter hole-saw and was cut using a band-saw to get 2 equal thickness, 74 mm diameter cylinders. Afterwards, these cylinders were router planed to 8 mm thickness to produce 10 radial and 10 tangential (in thickness direction) samples for determining transverse diffusivity. The side surfaces of all specimens were coated with two layers of epoxy resin to guarantee the air tightness of the lateral surfaces during measurement. In order to create a fresh flow through surface, these specimens were cleaned by air at pressure of 7 bar. The samples used for gas permeability were equalized in a conditioning chamber at 65 % ± 2 % relative humidity and 20 ºC ± 0,1 ºC temperature to produce equilibrium conditions of 12 % moisture content. The diffusivity

95 samples were equalized in another conditional chamber at 75 % ± 2 % relative humidity and 35 ºC ± 0,1
96 ºC temperature to meet 14 % moisture content.

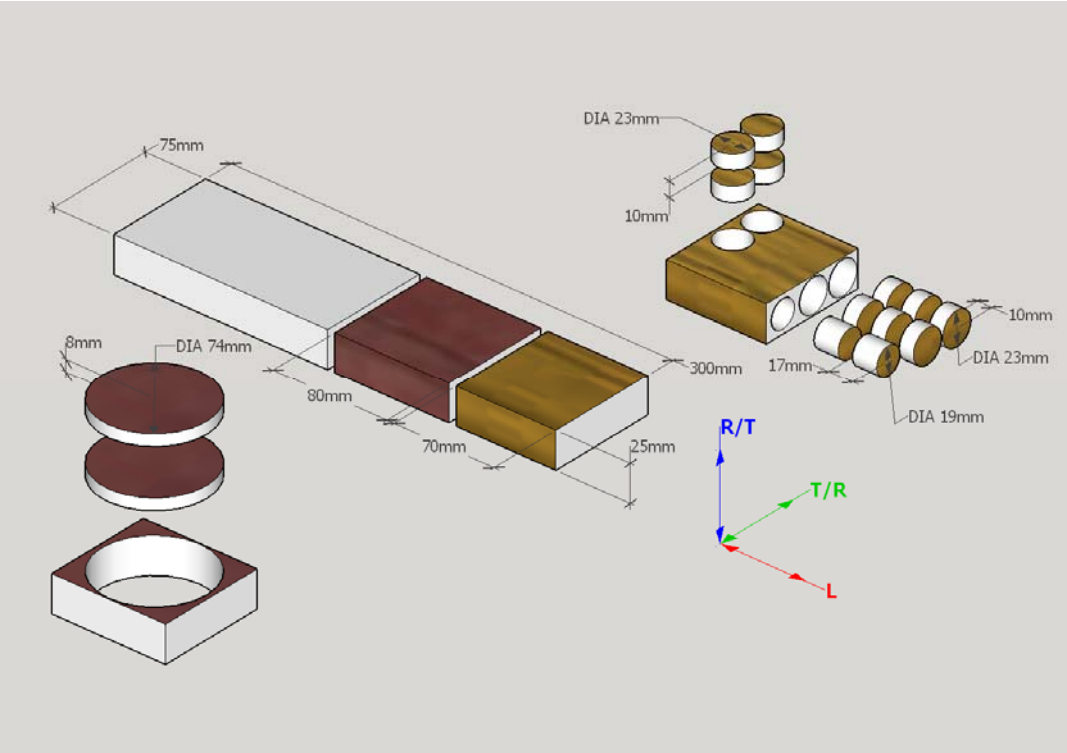

97

98 **Figure 1:** Sample preparation for permeability and diffusivity tests: foreground – longitudinal (L)
99 sampling, background – radial (R), and tangential (T) sampling.
100

101 **Methods**

102 **Permeability**

103 Permeability is the property of a material that indicates the ability of free fluids (gas and liquid) to flow
104 through them in response to a pressure gradient (Milota *et al.* 1995; Leggate *et al.* 2019). In previous
105 studies, gas and liquid permeability was measured by the rate of permeating flow of fluid through a
106 wood specimen of known length and cross-sectional area while a known pressure difference was applied
107 across it (Booker 1977; Leggate *et al.* 2019). It was calculated manually via the equation 1 by Darcy's
108 law (Redman *et al.* 2012):

$$K = \frac{Q\mu eP}{A\Delta P\bar{P}} \quad (1)$$

in which K is the intrinsic permeability (m^2)

Q is the fluid flux ($m^3 \cdot s^{-1}$)

μ is the dynamic viscosity of fluid ($Pa \cdot s$)

e is the sample thickness (m)

P is the pressure at which flux Q is measured (Pa)

A is the sample area (m^2)

$\Delta P = P_2 - P_1$ is pressure difference between the fluid outlet (P_2) and inlet (P_1) sides of the sample (Pa)

$\bar{P} = (P_1 + P_2)/2$ is the averaged pressure inside the sample (Pa).

In the present study, all measurements and calculations for all three directions permeability (longitudinal, radial and tangential) were carried out automatically on a Porolux 1000 Porometer (IB-FT GmbH, Berlin, Germany) (Figure 2) with control software. Two types of medium for permeability determination were gas (atmospheric air) and liquid (rain-water). For gas, atmospheric air pressure was increased to 4200 mbar. The gas permeability was measured at a pressure difference within this range. For liquid, rain-water pressure was increased and maintained at 2000 mbar for 0,5 min to measure the longitudinal permeability and at 4500 mbar for 30 min to measure the transverse permeability. Due to the low permeability encountered for transverse samples (no permeability values could be measured in the transverse direction), the pressure and measurement time were increased. Since temperature influences gas and liquid viscosity, it was taken into account during permeability calculations. The sample thickness was measured at three positions and then averaged to enter into the software along with ambient temperature before running tests. The 298,6 mm^2 sample area was a constant because all measurements used the same SH25 sample holder (Figure 3).

Figure 2: Photo of the Porolux 1000 Porometer used for permeability test: input of atmospheric air (1) to system at pressure of 7 bar, air pressure line (2) is from system to water tank (3) to apply water to the sample holder (4) in liquid permeability test or to the sample holder directly in gas permeability tests, balance (5) for water output weight connected to the computer, monitor (6) shows parameters and results of the measurement process, and the samples (7).

(1) (2)

Figure 3: Photo of the SH25 sample holder: integral parts (1), assembled holder (2).

Water-vapour diffusivity

Two commonly used methods for measuring diffusion coefficients are steady-state and unsteady-state which have different advantages and disadvantages. However, effects of vapour flow out of the sample surface in the steady-state measurement and the sample being exposed to the outside environment in the unsteady-state measurement should be eliminated (Perré 2007). To avoid complexity in this study, the steady-state method was used. The principle of measurement in the steady-state regime is based on the relationship between the partial pressure of vapour and the relative humidity at a fixed temperature. If two surfaces of a wood sample are exposed to two different relative humidity levels, the difference in vapour pressure happens. This is the driving force of the diffusive flux through the sample (Zohoun *et al.* 2003). The mass adsorbed or desorbed is weighed by the sample at chosen time intervals during the experiment to calculate the diffusion coefficient (Tagne *et al.* 2016).

In this study, the steady-state determination of water-vapour diffusivity was chosen and the technique of the vaporimeter was used (Figure 4). These experiments were performed on a vaporimeter that based on the PVC-CHA system developed by the team at AgroParisTech, France as described by Redman *et al.* (2012).

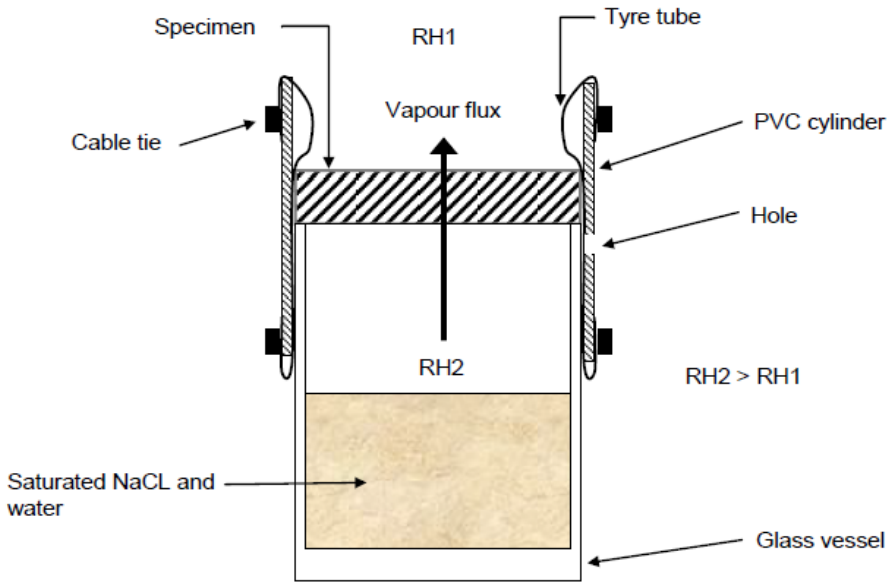

156

157 **Figure 4:** Vaporimeter based on the PVC-CHA system for water-vapour diffusivity test, in the weight
158 loss sequence (Redman *et al.* 2012).

159

160 As mentioned, before the experiment, wood samples were placed into the conditioning chamber to meet
161 14 % moisture content.

162 The 19 mm and the 74 mm diameter cylindrical samples were placed onto similar diameter glass vessels
163 containing a saturated solution of purified water and sodium chloride, ACS regent, ≥ 99,0 % to measure
164 the longitudinal and the transverse diffusivity respectively. A stable relative humidity (RH2) of 75 %
165 inside the vessel was produced from the saturated salt solution at 35 ºC. To create an airtight seal around
166 the sample and the vessel, a cylinder of PVC was used with an inserted piece of tyre tube clamped using
167 cable ties (Figure 5). The installation of the device into the PVC pipe required the assistance of a vacuum
168 pump to suck the tyre tube against the pipe wall while it was lowered over the sample and vessel. In the
169 absence of the vacuum, the tyre tube relaxes tightly to the sample and vessel, creating an airtight seal.

(1) (2)

Figure 5: Photo of vaporimeter for transverse (1) and longitudinal diffusivity test (2).

Aiming to create a vapour pressure gradient between two sides of the sample, the vaporimeter devices were placed in a constant environment chamber at 40 % relative humidity (RH1) and 35 ºC temperature, that produced equilibrium conditions of 7 % moisture content (Figure 6). This pressure gradient driving force created the diffusive flux through the sample during the measurement time. The diffusive flux was recognized by weighing the device periodically over time.

Figure 6: Photo of equipment to measure the mass flux in the steady-state regime.

The weight was carried out at the beginning of the measurement process but the mass flux of vapour (the overall weight loss) was only recognized when the decrease of mass was stable. A steady-state relationship was observed after a few days when the plot of the weight reduction as a function of time became a straight line.

By weighting the device inside the chamber via sealed glove gauntlets in the chamber door, and using a mass balance, accurate to 1 mg, placed inside the chamber (Figure 6), this experimental device allowed the mass flux to be measured with good stability of the conditions of temperature and relative humidity whatever the length of tests was.

The diffusion coefficient (D_b) is then calculated from the following formula (Redman *et al.* 2012),

$$D_b = \frac{mL}{tAG\rho_w \Delta X} \qquad (2)$$

in which D_b is the diffusion coefficient ($m^2 \cdot s^{-1}$)

m is the mass of transferred vapor (kg)

L is the sample thickness (m)

t is time (s)

A is the sample area (m^2)

G is the specific gravity of the sample at moisture content X. X is final moisture content of sample (%)

ρ_w is the density of water ($kg \cdot m^{-3}$), considered as 1000 $kg \cdot m^{-3}$

$\Delta X = (X_b+X_t)/2$ is the moisture content difference between the two parallel surfaces of the sample ($kg \cdot kg^{-1}$); X_b is the moisture content of the sample bottom ($kg \cdot kg^{-1}$), X_t is the moisture content of the sample top ($kg \cdot kg^{-1}$).

203 **Statistical Analysis**

204 The significant difference in permeability and diffusivity means between each pair of directions was
205 assessed by one-way analysis of variance (ANOVA). Comparision procedures were carried out at a
206 significance level (alpha) of 0,05. If the P-value in ANOVA results table was less than 0,05, the
207 difference in these means was significant.

208 Standard deviation (SD) was performed and presented with mean of data in tables.

209 **RESULTS AND DISCUSSION**

210 **Permeability**

211 Gas and liquid permeability data for *A. mangium* in the longitudinal, radial, and tangential directions
212 were presented in Table 1. The results highlighted the major difference between gas and liquid figures.
213 The gas permeability was 4, 23, and 74 times higher than the liquid permeability in the longitudinal,
214 radial, and tangential direction respectively. The difference between the gas and liquid permeability was
215 smallest in the longitudinal direction, but it was significant because the p-value was $5{,}67 \times 10^{-27}$, much
216 less than 0,05. These highly significant differences can be attributed to air being approximately 50 times
217 less viscous than water at room temperature and the lower molecular size of air compared with water.
218 Air is able to move through the small opening in wood tissue more easily than water. It is in agreement
219 with the results obtained by Taghiyari (2012).

220 **Table 1:** Longitudinal (L), radial (R), and tangential (T) gas and liquid permeability (K) and
221 anisotropy ratios for *A. mangium.*

Type	K (m^2)						Anisotropy Ratio		
	$Lx10^{-15}$		$Rx10^{-15}$		$Tx10^{-15}$		K_L/K_R	K_L/K_T	K_R/K_T
	Mean	SD	Mean	SD	Mean	SD			
Gas	2184,82	377,55	31,18	3,32	29,71	4,28	70,07	73,54	1,05
Liquid	539,11	174,87	1,36	0,13	0,40	0,06	396,68	1338,35	3,37

222

223 The results also showed the anisotropy ratios of both gas and liquid permeability. In previous studies,
224 the longitudinal permeability can be over 1 million times greater than the transverse permeability for
225 hardwoods (Agoua and Perré 2010; Redman *et al.* 2012). In this study, the longitudinal to tangential
226 anisotropy ratio in liquid permeability was highest, but it was about over 1 thousand. The longitudinal
227 to transverse anisotropy ratio in gas permeability was about 70. Except for the insignificant difference
228 in the gas permeability between the radial and tangential directions (p = 0,40), the differences in the gas
229 and liquid permeability between the other directions were highly significant (p-values were all from 10^{9}
230 to 10^{12} times less than 0,05). The radial liquid permeability was 3,37 times higher than the tangential
231 liquid permeability ($p = 2{,}91 \times 10^{-14}$). This might be explained by the radial liquid flow is predominately
232 through the ray, pit and cell wall capillary system, while the tangential liquid flow is more difficult to
233 go through the pit structure (Hansmann *et al.* 2002), where the bubbles are appeared to impede liquid
234 flow. This phenomenon is also used to explain the differences in the radial and tangential diffusivity
235 below. The high radial to tangential anisotropy ratio in liquid permeability is predicted to be one of the
236 causes of drying defects for *A. mangium*.
237 Table 2 shows gas permeability for other hardwood species published by Agoua and Perré (2010) and
238 Redman *et al.* (2012). Although their data were not results from parallel experiments with our
239 experiments, they were obtained by tests using the same methods, on the same equipment system (ALU-
240 CHA) and based on the same principle. All three measurement directions, longitudinal, radial and
241 tangential, were performed in all of experiments. Using a mass flow meter to measure the air flux and
242 calculating the permeability manually were differences in their studies compared to ours. However, this
243 was not a big problem because the experiments were conducted in the elimination of equipment factors
244 that could influence the results. *A. mangium* measured in this work was more permeable in all directions
245 than the highest published figure shown in Table 2. This suggests the high permeability of *A. mangium*

compared to other species reported partly relating to its fast drying rate at above fibre saturation point. The gas permeability anisotropy ratios were more modest in *A. mangium* than other species reported. This is probably due to the fact that the transverse pathways system (e.g. pits, rays) of *A. mangium* is more open.

Table 2: Longitudinal (L), radial (R), and tangential (T) gas permeability (K) and anisotropy ratios for other hardwood species.

Species	K (m^2)			Anisotropy Ratio		
	$Lx10^{-15}$	$Rx10^{-15}$	$Tx10^{-15}$	K_L/K_R	K_L/K_T	K_R/K_T
Spotted gum[b] (*Corymbia citriodora* Hook)	0,4	-	0,000003		4750	
Blackbutt[b] (*Eucalyptus pilularis* Sm)	35,0	0,00001	0,00002	2440000	2305000	0,9
Jarrah[b] (*Eucalyptus marginata* D.Don ex Sm.)	67,4	0,00005	0,00004	3005000	1531000	1,1
Messmate[b] (*Eucalyptus obliqua* L'Herit.)	55,5	0,0086	0,0003	16400	3086000	177
Beech[a] (*Fagus sylvatica*)	742	0,074	0,367	9970	2020	0,2
Teak[a] (*Tectona grandis*)	1750	0,00482	0,00569	363000	307000	0,8
[a] (Agoua and Perré 2010); [b] (Redman *et al.* 2012).						

Water-vapour diffusivity

Figure 7 showed the evolution of the measured mass loss relating to the time in the transverse and longitudinal directions for *A. mangium*. To correct the effect of the sample geometry without being disturbed by the difference between the transverse and longitudinal sample diameters and the slight variation of sample thickness, the mass loss was divided by the sample cross-sectional area and multiplied by the sample thickness. For each test, the flux was computed from the linear part of the curves. The line chart described two distinctive groups of curves, one of small slopes and the other of extensively bigger slopes. The group of big sloped curves represented fluxes of water-vapour through

261 samples in the longitudinal direction, and the group of small ones represented those through the radial
262 and the tangential directions.

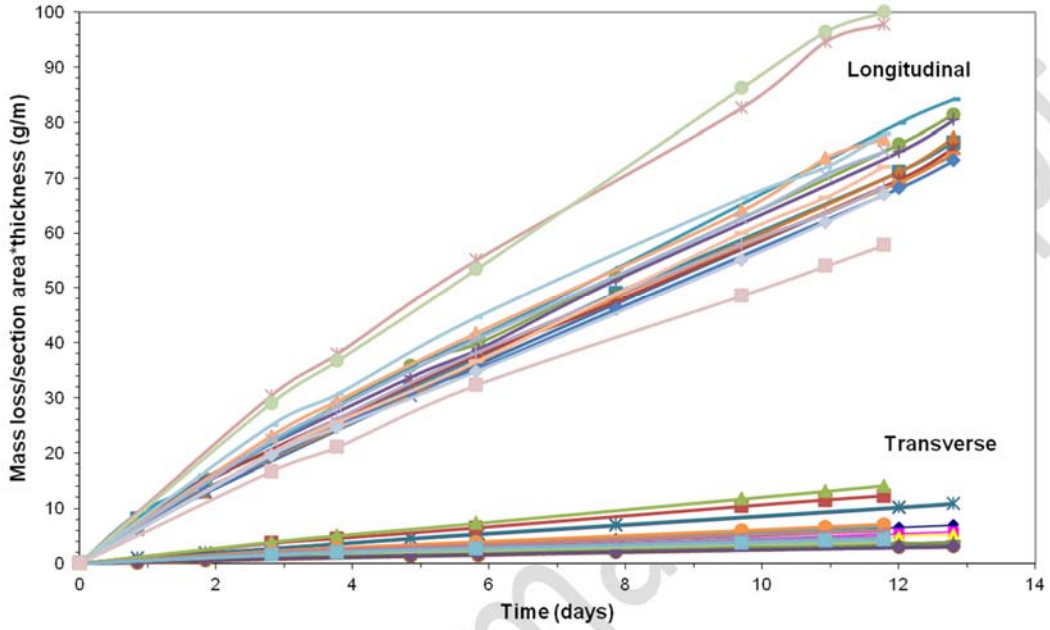

263

264 **Figure 7:** Evolution of the flux of bound water vapour over time in the R, T and L directions for *A.*
265 *mangium.*
266

267 The measured diffusion coefficients in the radial, tangential, and longitudinal directions for *A. mangium*
268 were presented in Table 3. The difference in the diffusivity between each pair of direction were highly
269 significant because p-values were all much less than 0,05. The highest p-value was $7{,}3 \times 10^{-4}$. The
270 obtained diffusion coefficients were in the range of 10^{-11} $m^2 \cdot s^{-1}$ to 10^{-9} $m^2 \cdot s^{-1}$ in the order of tangential,
271 radial to longitudinal direction. The longitudinal to transverse anisotropy ratios of diffusivity which were
272 in tens were much more modest than those of permeability. The radial diffusivity was 2,57 times higher
273 than the tangential diffusivity. Similar to the permeability, the variation of ray, pit and cell wall capillary
274 structures in the radial and tangential creating the difference in transverse diffusivity can also be a cause
275 of drying defects for *A. mangium*.

276

Table 3: Longitudinal (L), radial (R), and tangential (T) diffusion coefficients (D_b) and anisotropy ratios for *A. mangium.*

D_b (m^2 s^{-1})						Anisotropy Ratio		
$Lx10^{-10}$		$Rx10^{-10}$		$Tx10^{-10}$		D_{bL}/D_{bR}	D_{bL}/D_{bT}	D_{bR}/D_{bT}
Mean	SD	Mean	SD	Mean	SD			
13,73	2,67	1,33	0,62	0,52	0,12	10,34	26,62	2,57

The diffusion coefficients for other hardwood species published which were used to compare with *A. mangium* are shown in Table 4 (Agoua and Perré 2010; Redman *et al.* 2012). The numbers of all directions of diffusion coefficient for *A. mangium* were significantly higher than Australian hardwoods published by Redman *et al.* (2012), but markedly lower than two temperate hardwoods published by Agoua and Perré (2010). It is suggested that the drying rate from fibre saturation point of *A. mangium* can be faster than that of these Australian hardwoods, but slower than that of these temperate hardwoods. Besides, the higher radial to tangential diffusivity anisotropy ratio of *A. mangium* compounds its relatively easier drying defects at the late drying stage.

Table 4: Longitudinal (L), radial (R), and tangential (T) diffusion coefficients (D_b) and anisotropy ratios for other hardwood specie.

Species	D_b ($m^2 \cdot s^{-1}$)			Anisotropy Ratio		
	$Lx10^{-10}$	$Rx10^{-10}$	$Tx10^{-10}$	D_{bL}/D_{bR}	D_{bL}/D_{bT}	D_{bR}/D_{bT}
Spotted gum[b] (*Corymbia citriodora* Hook)	0,6	0,1	0,1	4,2	4,2	1,0
Blackbutt[b] (*Eucalyptus pilularis* Sm)	2,3	0,3	0,2	8,8	14,2	1,6
Jarrah[b] (*Eucalyptus marginata* D.Don ex Sm.)	2,7	0,3	0,4	10,5	7,2	0,7
Messmate[b] (*Eucalyptus obliqua* L'Herit.)	10,3	0,7	0,4	14,6	25,4	1,7
Beech[a] (*Fagus sylvatica*)	86	4,8	2,1	18,1	40,6	2,25
Teak[a] (*Tectona grandis*)	40	2,8	1,7	14,1	23,7	1,68
[a] (Agoua and Perré 2010); [b] (Redman *et al.* 2012).						

To summarize, results from this study suggested that the permeability and diffusivity of *A. mangium* were higher than other hardwoods published. By plotting permeability with diffusion coefficients, the demarcation between *A. mangium* and other materials were observed (Figure 8). Except for two temperate hardwoods reported by Agoua and Perré (2010), the *A. mangium* in both longitudinal and transverse directions were more permeable than all compared hardwoods and were more diffuse than the Australian hardwoods reported by Redman *et al.* (2012), which points out the fast and easy nature of removing water from *A. mangium* wood.

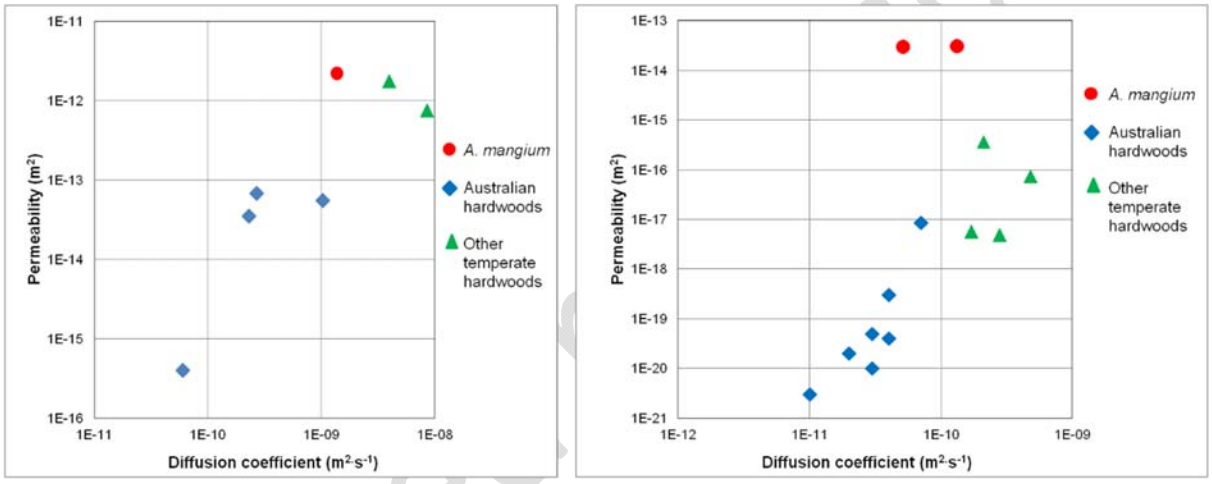

Figure 8: Comparison between permeability and diffusivity in the longitudinal (1) and transverse (2) directions for *A. mangium* and published hardwoods.

CONCLUSIONS

Characterization of mass transfer properties, gas and liquid permeability and diffusivity (in the steady-state regime) was achieved for *A. mangium* wood - a popular material supplying the wood industry in Vietnam. The results highlighted that:

- The gas permeability was significantly higher than liquid permeability in each direction. This difference increased respectively from the longitudinal, radial, to tangential direction.

- The permeability anisotropy ratios from longitudinal to transverse direction were not as so high as that of other species in previous reports. The radial to tangential anisotropy ratio was not significant in gas permeability, but quite high in liquid permeability.
- The measured mass losses over time in the transverse and longitudinal directions were plotted. There was an obvious distinction between groups of sloped curves. The big group was the water-vapour loss through the longitudinal direction and the small one was that of transverse directions.
- The longitudinal to transverse anisotropy ratios of diffusivity were much slighter than permeability. The difference between the radial and tangential diffusivity was significant, as same as for liquid permeability. This could be a cause of appearance of drying defects.
- By obvious demarcation on the mixed species graphs, the permeability and diffusivity in *A. mangium* were higher than other published hardwoods, which indicated a fast drying rate.

ACKNOWLEDGMENTS

The authors are grateful for the support of Research Institute of Forest Industries (RIFI) - Vietnamese Academy of Forest Sciences (VAFS) for the initial wood material collection; Salisbury Research Facility Center at the Department of Agriculture and Fisheries (DAF), Queensland, Australia is also acknowledged for assistance with labour and equipment. The authors thank to the Crawford Fund for the financial support of the training in relation to the activities of this study.

REFERENCES

Agoua, E.; Perré, P. 2010. Mass transfer in wood: Identification of structural parameters fromdiffusivity and permeability measurements. *J Porous Media* 13(11): 1017-1024. http://doi.org/10.1615/JPorMedia.v13.i11.80.

Booker, R.E. 1977. Problems in the measurement of longitudinal sapwood permeability and hydraulic conductivity. *NZ J Forestry Sci* 7(3): 297-306. http://www.scionresearch.com/__data/assets/pdf_file/0003/37479/NZJFS731977BOOKER297-306.pdf/.

De Jong, W.; Sam, D.D.; Hung, T.V. 2006. *Forest Rehabilitation in Vietnam Histories, realities and future*. Center for International Forestry Research (CIFOR). Bogor, Indonesia. http://www.cifor.org/publications/pdf_files/Books/BDeJong0601.pdf.

Hansmann, C.; Gindl, W.; Wimmer, R.; Teischinger, A. 2002. Permeability of wood - A review. *Wood Res-Slovakia* 47(4): 1-16. http://www.academia.edu/27225462/Permeability_of_wood_-_a_review.

Haque, M.N. 2002. Modelling of solar kilns and the development of an optimised schedule for drying hardwood timber. Ph.D. Thesis, University of Sydney. Sydney, Australia. http://ses.library.usyd.edu.au/handle/2123/581/.

Harwood, C.E.; Nambiar, S.E.K. 2014. *Sustainable plantation forestry in South-East Asia*. Australian Centre for International Agricultural Research (ACIAR). Canberra, Australia. http://aciar.gov.au/node/12221.

Leggate, W.; Redman, A.L.; Wood, J.; Baillères, H.; Lee, D.J. 2019. Radial Permeability of the Hybrid Pine (*Pinus elliottii* × *Pinus caribaea*) in Australia. *Bioresources* 14(2): 4358-4372. http://bioresources.cnr.ncsu.edu/resources/radial-permeability-of-the-hybrid-pine-pinus-elliottii-x-pinus-caribaea-in-australia.

Milota, M.R.; Tschernitz, J.L.; Verrill, S.P.; Mianowski, T. 1995. Gas permeability of plantation loblolly pine. *Wood Fiber Sci* 27(1): 34-40. http://wfs.swst.org/index.php/wfs/article/view/249.

Phonetip, K. 2018. Investigating optimized drying methods for Eucalyptus delegatensis using a solar kiln. Ph.D. Thesis, University of Melbourne. Melbourne, Australia. http://hdl.handle.net/11343/212529.

Redman, A.L.; Baillères, H.; Perré, P.; Carr, E.; Turner, I.W. 2017. A relevant and robust vacuum-drying model applied to hardwoods. *Wood Sci Technol* 51: 701–719. http://doi.org/10.1007/s00226-017-0908-7.

Redman, A.L.; Baillères, H.; Turner, I.W.; Perré, P. 2012. Mass transfer properties (permeability and mass diffusivity) of four australian hardwood species. *Bioresources* 7(3): 3410-3424. http://ojs.cnr.ncsu.edu/index.php/BioRes/article/view/BioRes_07_3_3410_Redman_Mass_Transfer_Properties_Australian_Hardwood.

Taghiyari, H.R. 2012. Correlation between gas and liquid permeability in some nanosilver-impregnated and untreated hardwood. *J Trop For Sci* 24(2): 249-255. https://www.frim.gov.my/v1/JTFSOnline/jtfs/v24n2/249-255.pdf.

Tagne, M.S.; Rémond, R.; Rogaume, Y.; Zoulalian, A.; Perré, P. 2016. Characterization of sorption behavior and mass transfer properties of four central Africa tropical woods: Ayous, Sapele, Frake, Lotofa. *Maderas-Cienc Tecnol* 18(1): 207-226. http://doi.org/10.4067/s0718-221x2016005000020.

366 **Tuan, H.C. 2014.** *Announced the current status of national forest in 2013*, M.o.A.a.R.D. (MARD) (ed.).
367 (Decision no. 3322/QD-BNN-TCLN), Hanoi, Vietman.
368 http://tongcuclamnghiep.gov.vn/Media/AuflaNews/Attachment/3322_Q%C4%90-BNN_TCLN.pdf.

369 **Tuan, H.C. 2020.** Announced the current status of national forest in 2019, M.o.A.a.R.D. (MARD) (ed.).
370 (Decision no. 1423/QD-BNN-TCLN), Hanoi, Vietman.
371 http://tongcuclamnghiep.gov.vn/content/uploads/files/Hie%CC%A3%CC%82n%20tra%CC%A3ng%2
372 0ru%CC%9B%CC%80ng%202019.pdf.

373 **Yuniarti, K.; Brodie, G.; Ozarska, B.; Harris, G.; Waugh, G. 2018.** A mathematical model for
374 moisture movement during continous and intermittent drying of *Eucalyptus saligna*. *EUR J Wood Wood*
375 *Prod* 76: 1165–1172. http://doi.org/10.1007/s00107-018-1296-x.

376 **Zohoun, S.; Agoua, E.; Degan, G.; Perré, P. 2003.** An experimental correction proposed for an
377 accurate determination of mass diffusivity of wood in steady regime. *Heat Mass Transfer* 39: 147-155.
378 http://doi.org/10.1007/s00231-002-0324-9.

379

380